atmosphere

Article

Characteristics of High-Latitude Climate and Cloud Simulation in Community Atmospheric Model Version 6 (CAM6)

Eun-Hyuk Baek [1], Jungeun Bae [2], Hyun-Joon Sung [2], Euihyun Jung [1], Baek-Min Kim [2,*] and Jee-Hoon Jeong [1,*]

[1] Faculty of Earth System and Environmental Sciences, Chonnam National University, 77 Yongbong-ro, Buk-gu, Gwangju 61186, Korea; eunhyuk2@jnu.ac.kr (E.-H.B.); 218854@jnu.ac.kr (E.J.)
[2] Department of Environmental Atmospheric Sciences, Pukyong National University, 45 Yongso-ro, Nam-gu, Busan 48513, Korea; caroong24@pukyong.ac.kr (J.B.); hjsung0522@pukyong.ac.kr (H.-J.S.)
* Correspondence: baekmin@pknu.ac.kr (B.-M.K.); jjeehoon@jnu.ac.kr (J.-H.J.)

Abstract: Many global climate models (GCMs) have difficulty in simulating climate variabilities over high northern latitudes. One of the main reasons is the inability of GCMs to simulate proper cloud fraction and the amount of liquid-containing cloud over the region. This study assessed the impact of cloud simulation in high latitudes by comparing the long-term parallel simulations of Community Atmosphere Model version 6 (CAM6) and CAM5, the previous version. The results show that the CAM6 simulation exhibits a considerable improvement in the Arctic, especially by reducing the cold bias of CAM5 throughout the year. Over the sub-Arctic region, however, CAM6 produces an excessive cold bias in summer and a warm bias in winter compared to the observation, which is closely related to the overestimation of cloud fraction and the amount of cloud liquid. In summer, the overestimation of the cloud in CAM6 tends to alleviate the cold bias compared to CAM5 due to an increase in downward longwave radiation over the high latitudes, while causing the excessive cold bias by blocking downward shortwave radiation over the sub-Arctic land area. In winter, when there is little incidence of shortwave radiation, the overestimation of the cloud in CAM6 increases the downward longwave radiation, which alleviates the cold bias in CAM5 over the Arctic but induces an excessive warm bias over the sub-Arctic land. The excessive cloudiness in CAM6 could weaken the high-latitude internal variability, exacerbating the deteriorating climate variability and long-term trend simulations in the region.

Keywords: CAM6; high latitudes; cloud; climate

check for updates

Citation: Baek, E.-H.; Bae, J.; Sung, H.-J.; Jung, E.; Kim, B.-M.; Jeong, J.-H. Characteristics of High-Latitude Climate and Cloud Simulation in Community Atmospheric Model Version 6 (CAM6). *Atmosphere* **2022**, *13*, 936. https://doi.org/10.3390/atmos13060936

Academic Editors: John Walsh, Uma S. Bhatt and Muyin Wang

Received: 11 May 2022
Accepted: 5 June 2022
Published: 9 June 2022

1. Introduction

The high latitudes and the Arctic are experiencing the most rapid warming compared to any other place on Earth due to the increasing emission of greenhouse gases [1,2]. The so-called Arctic of warming is caused by complicated climate feedback mechanisms such as sea ice–albedo feedback [3], water vapor and cloud feedback [4], and lapse-rate feedback [5]. In addition to its regional impacts, it is also responsible for global circulation change, such as the expansion of the jet stream center and the occurrence of Ural blocking [6], as well as extreme weather and climate events over mid-latitude continents [7–9]. Most global climate models (GCMs) are, however, still struggling to represent the high-latitude climate accurately. As a result, the inter-GCM spread of the global warming scenario is the largest over the Arctic and the high latitudes [10–12]. Previous research has reported that such poor simulation of high-latitude climate in GCMs is associated with the shortwave (SW) and longwave (LW) radiation biases at the surface, which are linked tightly to the cloud simulation properties of the model [13–15].

Over the high latitudes, most GCMs underestimate the cloud fraction [11,14,16,17] and cloud liquid mass [17–19]. Less cloud fraction and cloud liquid mass lead to a weaker cloud radiative effect (CRE), producing a cold bias in GCMs compared to the observation.

Community Atmospheric Model version 5 (CAM5) [20], one of the most widely used climate models in climate research, also tends to simulate less cloud fraction and cloud liquid mass over the Arctic and high latitudes. Baek et al. (2020) [15] suggested that this is partly explained by the lesser supply of moisture and heat from outside of the Arctic. Due to the deficiency in the simulations of cloud fraction and cloud liquid mass in the Arctic, CAM5 suffers negative surface air temperature (SAT) bias throughout the year. Some studies discovered that the cloud fraction and cloud liquid amount are sensitive to the perturbation magnitude on the Wegener–Bergeron–Findeisen (WBF) process [21,22]. They suggested that a better representation of the WBF process can improve the Arctic cloud simulation. Recently, CAM5 was updated to its new version, CAM6, which included new cloud physics parameterizations [23]. Danabsoglu et al. (2019) [23] demonstrated that CAM6 contains many substantial scientific and infrastructure improvements, as well as new capabilities, resulting in improved historical simulations compared to CAM5 and to available observations. McIlhattan et al. (2020) [24] reported that Arctic cloud liquid had increased dramatically from CAM5 to CAM6, which led to an increase in mean downwelling longwave and an increase in SAT over the Arctic using their preindustrial control runs. However, their study focused on the preindustrial period and analyzed it over the limited domain confined to the Arctic region.

To examine the characteristics of clouds and their impact on the climate simulated by CAM6 over the high northern latitudes in present-day climate simulation in this study, Atmospheric Model Intercomparison Project (AMIP)-type simulations using both CAM5 and CAM6 were performed. By comparing the two simulations, we elucidate (1) the differences in the climate and cloud characteristics between CAM6 and CAM5 over the high latitudes and (2) the impacts of simulated cloud properties on the high-latitude climate simulation. Section 2 describes the model design and data used in this study. Section 3 presents the results, and Section 4 provides a summary and discussion.

2. Methods

2.1. Model and Experimental Design

As a successor to CAM5, CAM6 uses the same Finite Volume (FV) dynamical core as CAM5, but with significant changes in physical parameterizations [23]. One of the most important changes is the inclusion of the unified turbulence scheme Cloud Layers Unified By Binormals (CLUBB) [25]. CLUBB unifies the processes of cloudy turbulent layers by directly replacing the separate shallow convection boundary layer, and grid-scale condensation schemes (i.e., cloud macrophysics scheme) presented in CAM5 [26]. It is a high-order closure representation of moist turbulence that closes many terms by a novel use of a simple, multivariate binormal probability density function (PDF) describing subgrid-scale variations in temperature, humidity, and vertical velocity. Another important change is that the Morrison–Gettelman cloud microphysics scheme (MG1) [27] in CAM5 has been replaced by an updated version (MG2) [28], which is able to forecast, instead of diagnose, the mass and number concentration of falling condensed species (i.e., rain and snow). Additionally, there were some changes in various physics parameterizations, such as Modal Aerosol Model version 4 (MAM4) [29] and orographic gravity wave drag parameterization [30]. Previous studies reported that the primary changes in cloud physics parameterizations in CAM6 lead to an increase in cloud fraction and cloud liquid amount over the Arctic [24].

To evaluate the impact of physical parameterization changes in cloud simulation and associated high-latitude climate from CAM5 to CAM6, we conducted AMIP simulations with CAM5 and CAM6 for 36 years, from January 1979 to February 2015, with a horizontal resolution of 1.9° latitude × 2.5° longitude and with 30 vertical layers. Both simulations were run with five ensembles and used the same observed monthly mean SST and sea ice concentration data from the HadOI products [31]. We compared the ensemble-averaged monthly climatologies of the two simulations. The model cloud fraction was calculated using the lidar simulator in the Cloud Feedbacks Model Intercomparison Project (CFMIP)

Observation Simulator Package (COSP) diagnostic model for comparison with satellite observation data. A detailed description of the COSP diagnostic model can be found in Shaw et al. (2021) [32].

2.2. Observational Data

The observed cloud fraction was obtained from the Cloud–Aerosol Lidar and Infrared Pathfinder Satellite Observations (CALIPSO)–GCM Oriented CALIPSO Cloud Product (CALIPSO–GOCCP) from June 2006 to February 2015 [33]. CALIPSO, an active remote sensing satellite, is specifically well adapted for observing (i) clouds with optical depth lower than 3, (ii) sparse clouds such as shallow cumulus, and (iii) occurrence of clouds within the first 2 km above the surface (continent and ocean) [16]. Thus, CALIPSO–GOCCP currently provides the best satellite observations of high-latitude clouds because it can detect optically thin clouds without relying on the albedo or thermal contrast [16,34]. The climatology data of long-term ground-based cloud and radiation measurements from 1998 to 2010 at the North Slope of Alaska (NSA) Barrow site (71.38° N, 156.68° W) from the Atmospheric Radiation Measurement (ARM) Best Estimate (ARMBE) dataset [35] were used for the model evaluation. The high-latitude SAT, downward SW radiation at the surface (FSDS), downward LW radiation at the surface (FLDS), and cloud condensate mass were obtained from the European Center for Medium-Range Weather Forecasts (ECMWF) ERA-Interim reanalysis dataset from January 1979 to February 2015 [36].

3. Results

In terms of annual averages, both models simulate the spatial SAT pattern reasonably well over the high latitudes (Figure 1a–c) with CAM5; however, they exhibit a cold bias compared to observations in most high latitudes. The bias is large up to 5 K over the Arctic, as reported in previous studies [15] (Figure 1d). CAM6 shows noticeable improvements in the climate simulation over the high latitudes and the Arctic (Figure 1f). The most notable one is that the cold bias in the Arctic has almost disappeared in CAM6. However, when looking at the summer (JJA) and winter (DJF) averages in Figure 2, the removal of this bias shows a different pattern in the Arctic and sub-Arctic continents. In summer, CAM5 shows a relatively weak cold bias over the Arctic and a weak warm bias over the sub-Arctic continent (Figure 2a). CAM6 simulates the warmer Arctic, alleviating the cold bias (Figure 2b). Over the sub-Arctic continents, in contrast, CAM6 simulates colder temperatures than CAM5, showing a rather cold bias with respect to the observation (Figure 2c). The magnitude of the bias in CAM6 is somewhat larger than that of CAM5 (Figure 2a,c). In winter, CAM5 shows a cold bias over the Arctic and the high latitudes. Similar to the annual mean bias pattern (Figure 1d), the cold bias is most significant over the central Arctic Ocean and the Canadian Archipelago. However, the sub-Arctic cold bias is also not negligible (Figure 2d). CAM6 simulates significantly warmer than CAM5 over most Arctic and sub-Arctic continents, such as northern Eurasia and northern Canada (Figure 2e). This effectively reduces the large cold bias of CAM5 over the Arctic region, which is the most noticeable improvement of CAM6 over CAM5. However, in the northernmost part of Eurasia, CAM6 exhibits a warm bias instead. Thus, the relatively weak bias of the annual mean SAT over the sub-Arctic continents in CAM6 (Figure 1f) can be considered as the result of offsetting the bias, showing different signs in summer and in winter.

To investigate the peculiar nature of this seasonal contrast of model bias of CAM6, we further examined the cloud and related climate variables over the Arctic (marked circle in Figure 2c,f, north of 70° N) and the Northern Eurasian continent (the marked trapezoid in Figure 2c,f, longitude 60° E~150° E, latitude 55° N~70° N), which is denoted as sub-Arctic in Figures 3, 5, 8 and 9). We focused on the changes in the cloud amount over the denoted regions because both LW and SW CRE are essentially important in determining the high-latitude SAT. Over the Arctic and sub-Arctic region, the increase in summer clouds has a net cooling effect because the SW blocking effect is much larger than the LW reflection effect [37]. In contrast, the increase in clouds in winter when there is little incident

SW radiation leads to a net warming effect because of the increase in downwelling LW radiation.

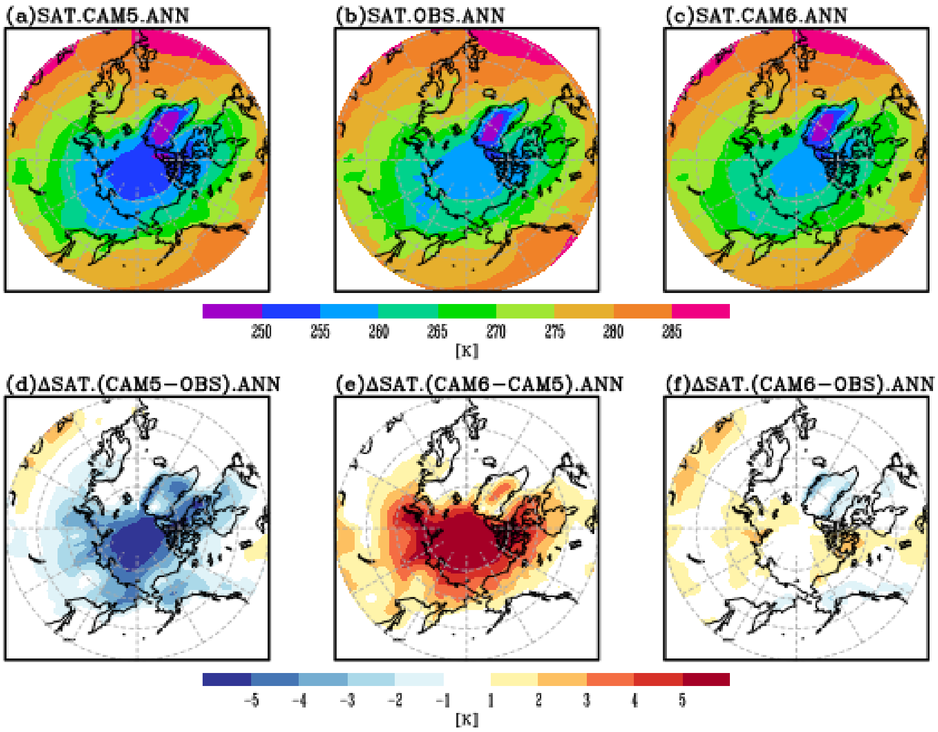

Figure 1. Annual mean surface air temperature (SAT) of (**a**) CAM5 simulation, (**b**) ERA-Interim reanalysis, and (**c**) CAM6 simulation. Biases of the SAT against the reanalysis were obtained from (**d**) CAM5 and (**f**) CAM6, and (**e**) the differences in SAT between CAM6 and CAM5.

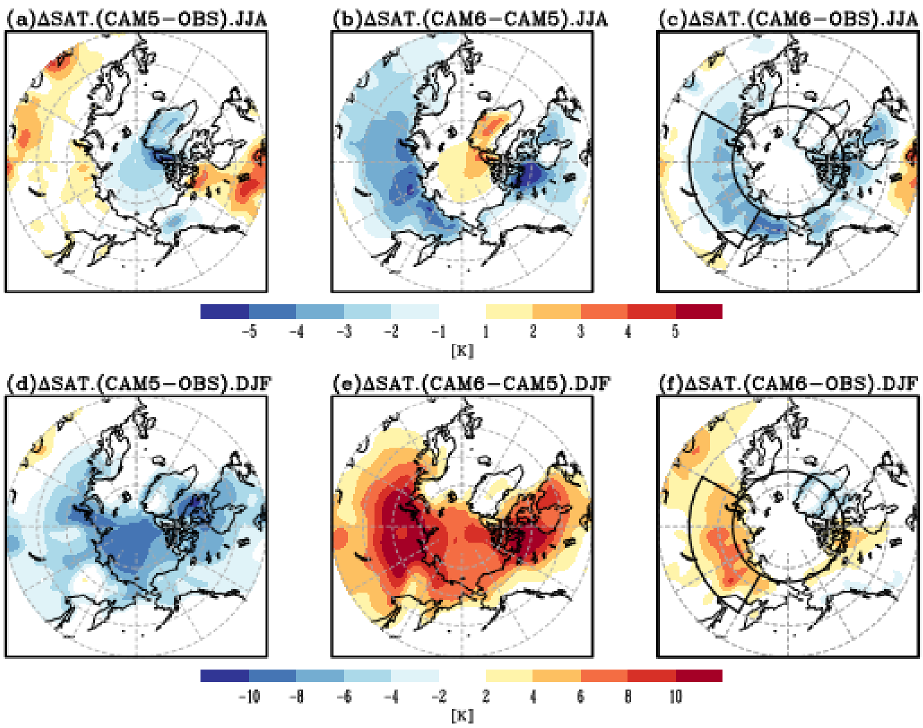

Figure 2. Biases of surface air temperature (SAT) against the ERA-Interim reanalysis during (**a**–**c**) JJA and (**d**–**f**) DJF obtained from (**left**) CAM5 and (**right**) CAM6, and (**center**) the differences in each variable between CAM6 and CAM5.

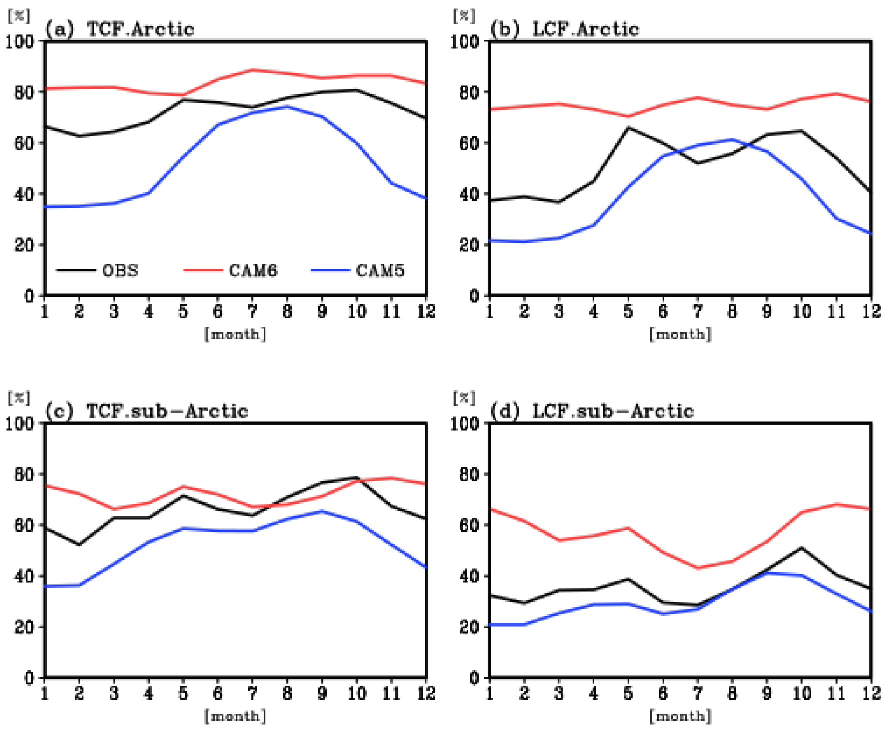

Figure 3. Annual cycles of the (**a**) total cloud fraction (TCF) and (**b**) low cloud fraction (LCF) averaged over the Arctic from CALIPSO–GOCCP observations averaged from June 2006 to November 2010 (black line), CAM6 (red line), and CAM5 (blue line). The CALIPSO–GOCCP observations were averaged from June 2006 to February 2015, and the model results are the means of AMIP simulation results for 36 years, from January 1979 to February 2015. (**c**,**d**) are the same as (**a**,**b**), except for over the sub-Arctic area.

Figure 3 shows the simulated cloud fraction in CAM5 and CAM6 together with satellite observation values. As reported in previous studies [15], the simulated total cloud fraction (TCF) over the Arctic in CAM5 is smaller than that of CALIPSO–GOCCP satellite observation throughout the year. This tendency is more prominent, especially in winter (Figure 3a). The lower cloud fraction (LCF), which greatly influences the radiative process, has a similar pattern to TCF but represents a weak overestimation in summer (Figure 3b). Conversely, CAM6 overestimates TCF and LCF compared to observations over the Arctic throughout the year (Figure 3a,b). It is noteworthy that CAM5 exhibits seasonal variation similar to that observed in the Arctic, while CAM6 overestimates both TCF and LCF compared to the observation in winter, which fails to represent seasonal variability. Over the sub-Arctic, similarly, CAM5 (CAM6) underestimates (overestimates) the cloud fraction compared to the observation (Figure 3c,d). Over the sub-Arctic region, CAM6 overestimates by above 10% in summer and by about 30% in winter. In summary, CAM6 simulates a considerably larger cloud fraction than CAM5 over the Arctic and the high latitudes throughout the year, which even causes an excessive overestimation compared to observation. The increase in the cloud fraction of CAM6 can further increase CRE compared to CAM5 over the region. Not only the biases against satellite observation but also the biases against Arctic ground-based observation show similar characteristics between the two models. Figure 4 shows the annual cycles of TCF, liquid water path (LWP), FSDS, and FLDS from CAM5, CAM6, and the observations at the Barrow site. The TCF is less in the CAM5 results than in the observations, except in July and August. The LWP is also underestimated over the entire period. Accordingly, the FSDS is overestimated and the FLDS is underestimated, particularly in autumn and winter. In contrast, the TCF and the LWP in CAM6 are overestimated compared with the observations over the entire period, which causes the underestimation of the FSDS in summer and the overestimation of the FLDS in winter.

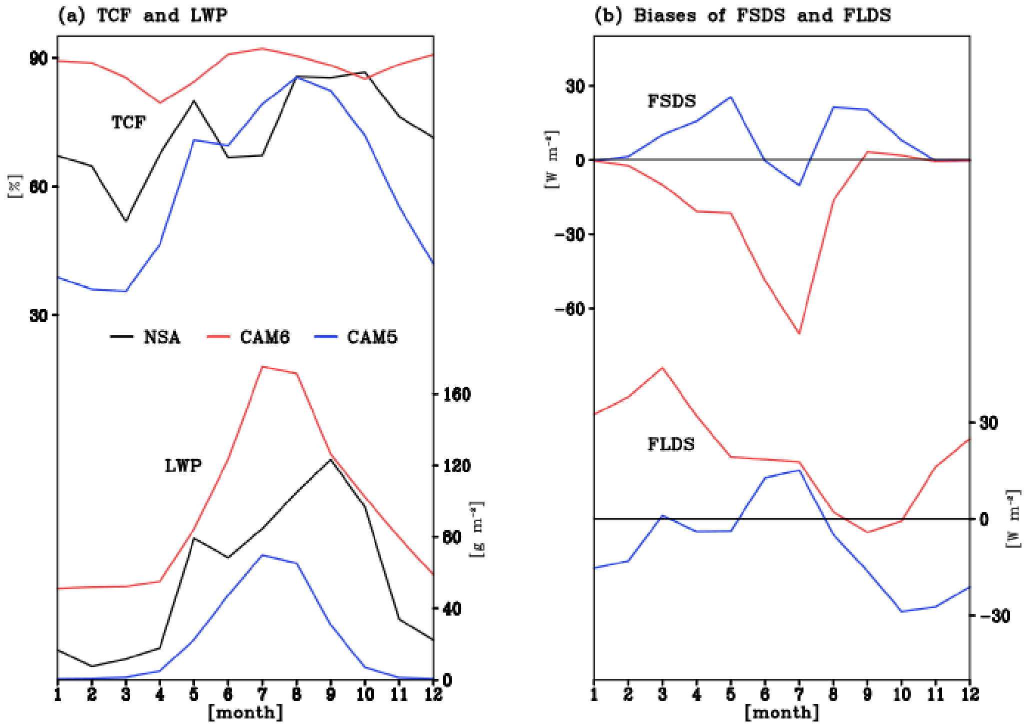

Figure 4. Annual cycles of total cloud fraction (TCF), upper part in (**a**) and liquid water path (LWP), bottom part in (**a**) from the climatology of ground-based cloud and radiation measurements at the North Slope of Alaska (NSA) Barrow site (black line), CAM6 (red line), and CAM5 (blue line). Biases of surface downward SW flux (FSDS), upper part in (**b**) and surface downward longwave flux (FLDS), bottom part in (**b**) of SAM0 (red line) and CAM5 (blue line) against the climatology of ground-based cloud and radiation measurements at the NSA Barrow site.

Figure 5 shows the vertical profiles of the annual mean total cloud condensate, cloud liquid, and cloud ice simulated by CAM5/CAM6 and ERA-Interim reanalysis over the Arctic and the sub-Arctic. CAM5 simulates less total cloud condensates than that of the reanalysis over the Arctic both for cloud liquid and cloud ice. In particular, the underestimation of cloud liquid amount is larger than that of cloud ice; that is, the simulated cloud liquid (ice) amount is about one-seventh (one-fourth) less than the reanalysis, respectively. This result is consistent with that of previous studies which show that CAM5 underestimates supercooled liquid-containing clouds [15,34], and this shortcoming is similarly found by many other GCMs [18,38]. Macilhattan et al. (2020) reported that CAM6 produces more cloud liquid and less cloud ice than CAM5, which indicates that the mixed-phase clouds increase [24]. Our results also indicate that the amount of cloud liquid (ice) simulated in CAM6 is more (less) than in CAM5. The ratio of the mixed-phase clouds in CAM6 is even larger than the observation (not shown). Because of the overestimation of the cloud liquid amount in CAM6, the total cloud condensate is also overestimated compared to the reanalysis. The simulated cloud characteristics of CAM6 over the sub-Arctic are similar to those of the Arctic. Notably, CAM5 simulates a similar cloud liquid amount to the reanalysis over the sub-Arctic region. The increase in the ratio of cloud liquid amount over the Arctic and the high latitudes increases the cloud optical depth, which can increase CRF.

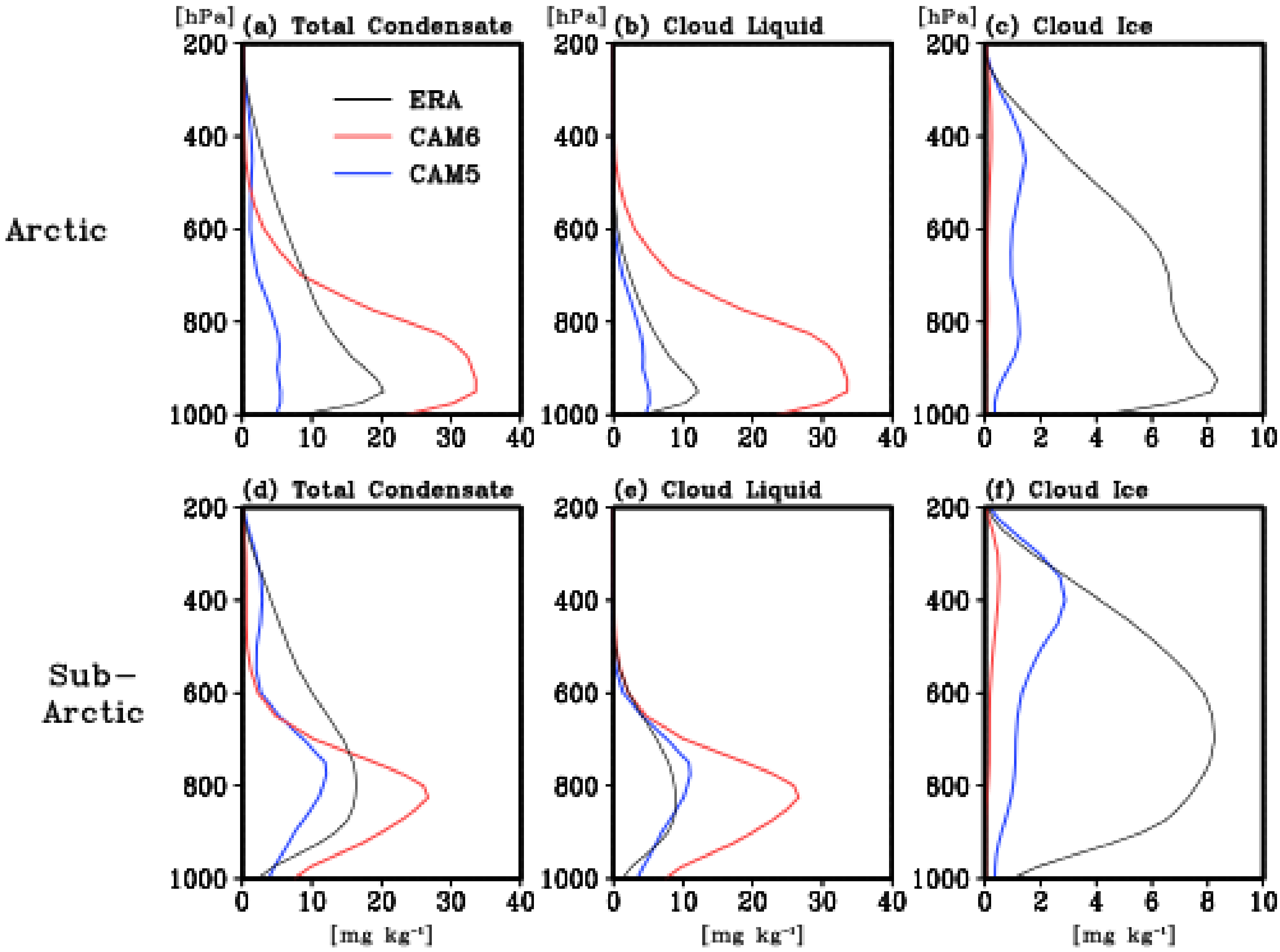

Figure 5. Annual mean vertical profiles of grid-mean (**a**) cloud condensate mass (cloud liquid + cloud ice), (**b**) cloud liquid mass, and (**c**) cloud ice mass averaged over the Arctic from ERA-Interim reanalysis (ERA, black lines), CAM6 (red lines), and CAM5 (blue lines). (**d**–**f**) are the same as (**a**–**c**) except for over the sub-Arctic area.

Figure 6 shows the bias of LCF, downward longwave radiation at the surface (FLDS), downward shortwave radiation at the surface (FSDS), and SAT, as well as the differences between the two models in summer. CAM5 underestimates LCF compared to the observations over the Arctic, Greenland, and Central Siberia, while it overestimates it in East Siberia and Alaska (Figure 6a). The reduction in Arctic clouds in CAM5 slightly decreases FLDS and strongly increases FSDS (Figure 6d,g). Although the bias in the FSDS is larger than that of the FLDS, the CRE by FSDS is very small because of the high surface albedo on sea ice over the Arctic. Then, the sum of the CREs by FLDS and FSDS causes a weak cold bias over the Arctic (Figure 6j). Compared to CAM5, CAM6 simulates a substantial increase in LCF over the Arctic and the high latitudes, which leads to Arctic warming due to the increase in FLDS and to the sub-Arctic cooling due to the decrease in FSDS (Figure 6b,e,h,k). Compared with the observation, the change in CAM6 substantially reduced the bias of FLDS in the Arctic. Meanwhile, excessive cloud overestimation enhances the reduction in FSDS and causes cold bias over the sub-Arctic region (Figure 6c,f,i,l).

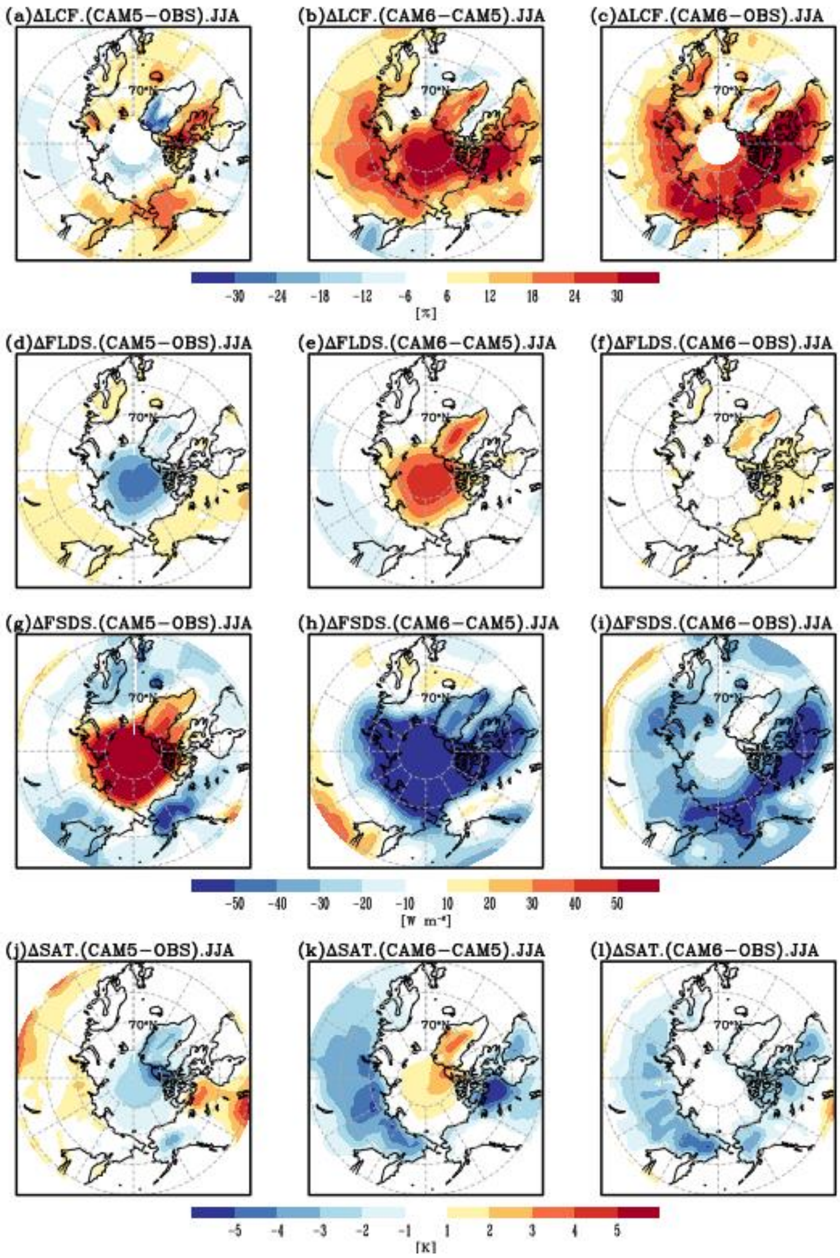

Figure 6. Biases of (**a**–**c**) low cloud fraction (LCF) against the CALIPSO–GOCCP observation, (**d**–**f**) downward longwave (LW) radiative flux at the surface (FLDS), (**g**–**i**) downward shortwave (SW) radiative flux at the surface (FSDS), and (**j**–**l**) surface air temperature (SAT) against the ERA-Interim reanalysis during JJA obtained from (**left**) CAM5 and (**right**) CAM6, and (**center**) the differences in each variable between CAM6 and CAM5.

As mentioned above, CRE by FLDS is dominant in determining SAT over the high latitudes, and SW radiation is almost zero in winter. Figure 7 shows the deviations in LCF, FLDS, and SAT from observations and the differences between the two models in wintertime. CAM5 underestimates LCF over all the high latitudes compared to the observation, which causes a decrease in the FLDS and a cold bias at the surface (Figure 7a,d,g). CAM6 produces a larger LCF than CAM5, which leads to an increase in both the FLDS and SAT (Figure 7b,e,h). This increase in LCF in CAM6 causes excessive overestimation of the LCF and FLDS compared to the observation. The excessive CRE by FLDS successfully reduces the cold bias over the Arctic but causes warm bias over the sub-Arctic region compared to the observation (Figure 7c,f,i). Our results reveal that the spatial pattern of the difference in the downwelling cloud radiation between the two models is consistent with that of SAT. The magnitude of the radiation strength is also large enough to affect SAT changes in both summer and winter. Consequently, the increase in cloudiness in CAM6 is responsible for improving the Arctic climate simulation and the degradation of the sub-Arctic climate simulation.

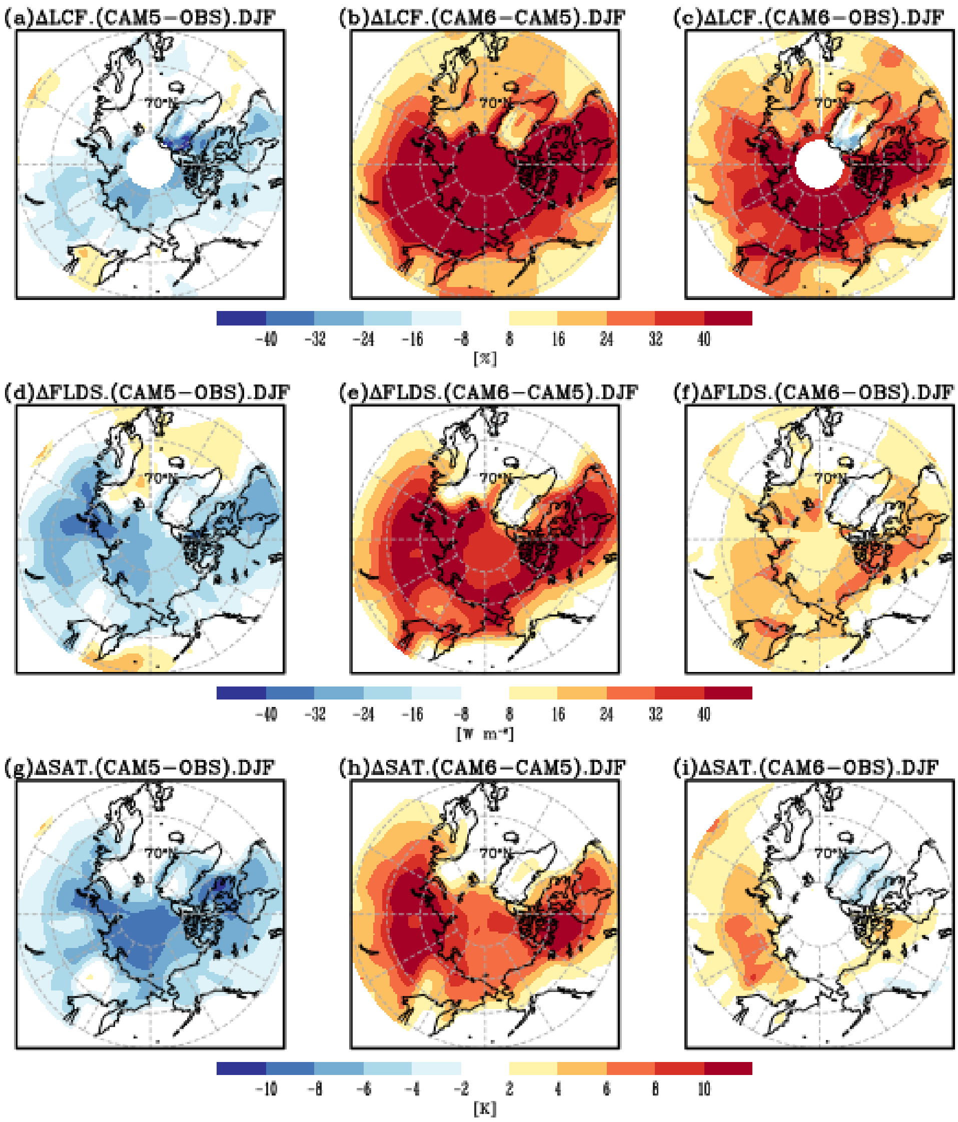

Figure 7. Biases of (**a**–**c**) low cloud fraction (LCF) against the CALIPSO–GOCCP observation, (**d**–**f**) downward longwave (LW) radiative flux at the surface (FLDS), (**g**–**i**) surface air temperature (SAT) against the ERA-Interim reanalysis during DJF obtained from (**left**) CAM5 and (**right**) CAM6, and (**center**) the differences in each variable between CAM6 and CAM5.

CAM6 simulates interannual variability and linear trends of the high-latitude climate differently from CAM5. Figure 8 shows the interannual variation of the annual and seasonal mean SAT over the Arctic and sub-Arctic region. Over the Arctic, as discussed above, CAM6 reduces the cold bias of CAM5 during the analysis period (i.e., 34 years) in both summer and winter, simulating the annual mean SAT similar to the observation. The magnitude of interannual variability of annual mean SAT in CAM6 is relatively small, unlike CAM5 and the observation mainly due to small interannual variability in the summertime. Both models simulate a weaker Arctic warming trend than the observed, especially in winter. Over the sub-Arctic region, CAM5 represents a weak warm bias in the summertime and a strong cold bias in the wintertime. In contrast, CAM6 produces a robust cold bias in the summertime and a robust warm bias in the wintertime continuously during the analysis period. The magnitudes of interannual variability in CAM6 are smaller than that of CAM5 and the observation for both of the two seasons. The linear trend of annual mean SAT simulated in CAM5 is similar to the observation, whereas CAM6 overestimates instead, especially in the summertime. Both models show a warming trend in winter, whereas observation shows a cooling trend. The characteristics of interannual climate variability simulated in both models are closely related to cloud simulation. Figure 9 shows the interannual variation in the seasonal mean SAT and LCF over the Arctic and sub-Arctic regions. In both models, the correlation between the interannual variabilities in the SAT and LCF is significantly high, except for the summer Arctic, where the CRFs of LW and SW are combined. The magnitude of LCF's interannual variability in CAM6 is smaller than that in CAM5 in the Arctic and sub-Arctic summer and in the sub-Arctic winter. That seems to make the magnitudes of SAT's interannual variability in CAM6 small compared to CAM5. Consequently, the excessive cloudiness in CAM6 induces low interannual variability, which impairs the simulation performance of climate variability and trend over the sub-Arctic region.

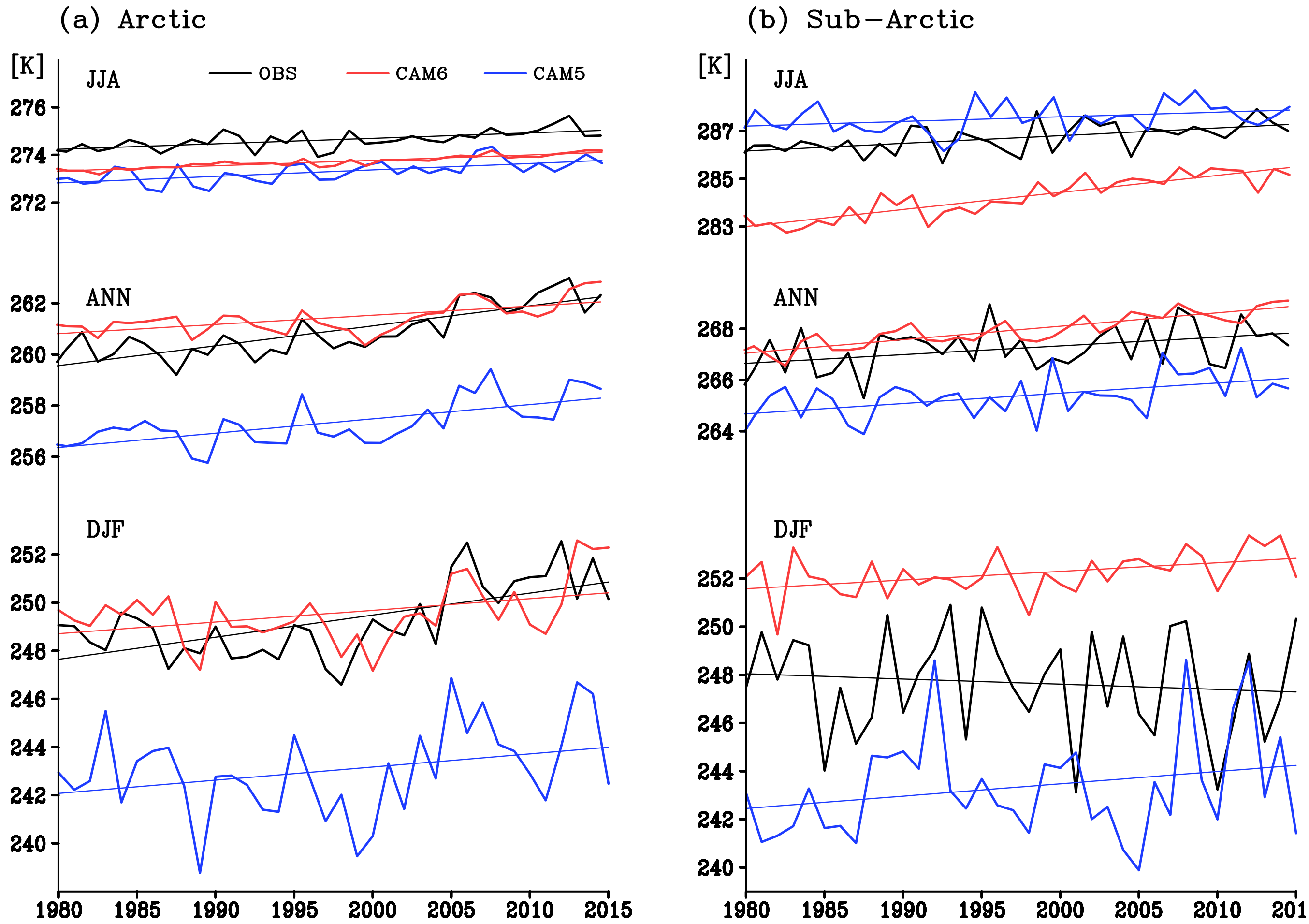

Figure 8. Interannual time series of the surface air temperature (SAT) averaged over (**a**) the Arctic and (**b**) sub-Arctic during (**upper**) JJA, (**middle**) annual mean, and (**bottom**) DJF from ERA-Interim reanalysis (ERA, black lines), CAM6 (red lines), and CAM5 (blue lines). The solid thin lines indicate their linear trend.

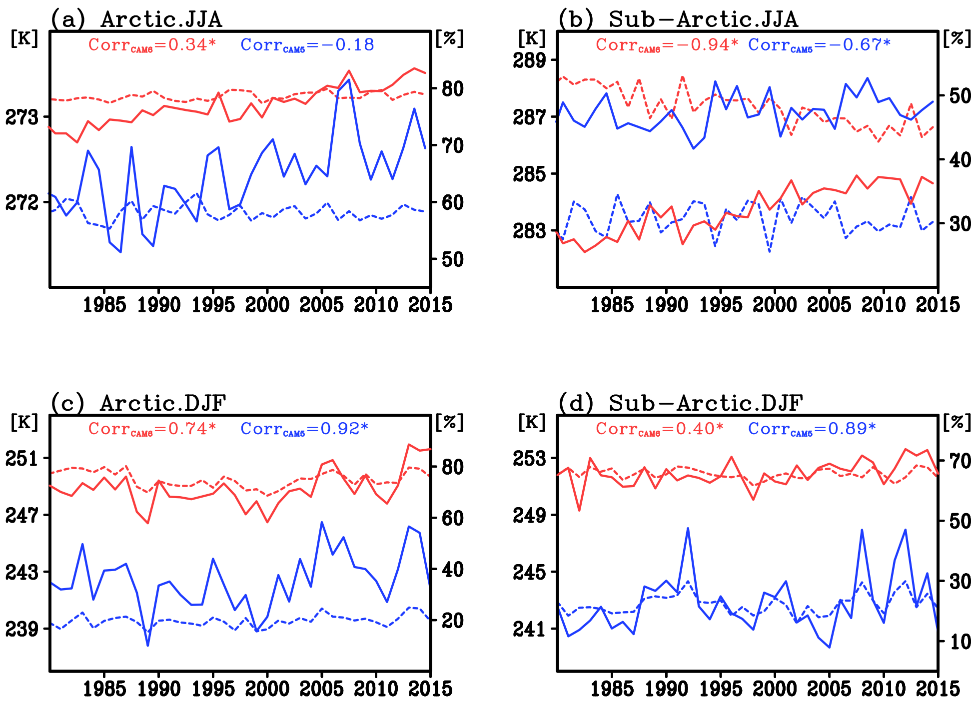

Figure 9. Interannual time series of the surface air temperature (SAT, solid line) and low cloud fraction (LCF, dotted line) averaged over (**a**,**c**) the Arctic and (**b**,**d**) the sub-Arctic region during (**a**,**b**) JJA and (**c**,**d**) DJF from CAM6 (red lines) and CAM5 (blue lines). "$Corr_{XX}$ = XX" indicates the correlation between SAT and LCF for CAM6 (red) and CAM5 (blue). The asterisks indicate statistical significance ($p < 0.05$).

4. Summary and Discussion

Many GCMs have difficulty simulating climate and clouds over the Arctic and the northern high latitudes. This study assessed the impact of cloud simulation in high latitudes by comparing the long-term parallel simulations of CAM6, the latest version, and CAM5, the previous version. The results show that CAM6 represents a considerable improvement over the Arctic in reducing the cold bias of CAM5 throughout the year. In contrast, over the sub-Arctic region, CAM6 simulates larger biases of SAT and clouds than that of CAM5 in producing an excessive cold bias in summer and an excessive warm bias in winter. Although the characteristics of high-latitude climate simulation in CAM6 vary according to seasons and regions, there is one cause: CAM6 simulates more cloud fraction and cloud liquid amount than CAM5 both over the Arctic and the sub-Arctic areas throughout the year. In particular, the cloud fraction simulated in CAM6 does not represent seasonal variability, unlike CAM5 and the observation, which causes a considerable overestimation of the winter cloud fraction compared to the observation. Previous studies noted that the increases in cloud liquid amount over the high latitudes in CAM6 are mainly due to two updated physical parameterizations: a mixed-phase ice nucleation scheme and a new version of the microphysics package (MG2) [39]. The new mixed-phase ice nucleation scheme implies that in relatively clean air, such as the one above the Arctic, ice nucleation and cloud ice formation are limited [40]. The prognostic precipitation in MG2 reduces the precipitation frequency in the liquid cloud over the high-latitudes [24]. The two physical parameterizations in CAM6 may enhance to increase the cloud liquid relative to CAM5.

The increases in the cloud fraction and the cloud liquid amount enhance CRF over the high latitudes. In the summer, the overestimation of the cloud amount in CAM6 alleviates the cold bias in CAM5 increasing FLDS in the Arctic, but it causes an excessive cold bias by blocking FSDS over the sub-Arctic land area. In winter, the overestimation of the cloud amount in CAM6 alleviates the cold bias in CAM5 over the Arctic, increasing FLDS, but induces the excessive warm bias over the sub-Arctic land area. In addition, the excessive cloudiness in CAM6 causes low interannual variability, which impairs the simulation performance of climate variability and trends over the sub-Arctic region. The characteristics of high-latitude climate and cloud simulation in CAM6 should be considered when interpreting the various results of climate experiments using CAM6. Not only the climate simulation but also the increase in the cloud fraction and cloud liquid amount over the Arctic may be responsible for the sea ice simulation in fully coupled GCM. Huang et al. (2021) [41] examined this issue using Community Earth System Model version 1(CESM1), whose atmospheric component is CAM5. They demonstrated that the increase in the cloud fraction and cloud liquid amount enhances melting sea ice over the North Atlantic Ocean, most likely caused by a positive feedback process between clouds, radiation, and sea ice. Our further study will address this issue using CESM2 including CAM6.

Author Contributions: E.-H.B., J.B., H.-J.S. and E.J. performed the overall numerical experiments and analysis. B.-M.K. and J.-H.J. designed the project and helped analyze the simulation results and the observations. All authors have read and agreed to the published version of the manuscript.

Funding: This work was supported by the National Research Foundation of Korea Grant funded by the Korean Government (NRF-2019R1I1A1A01061694). B.-M.K. is supported by the Korea Meteorological Administration Research and Development Program (grant No. KMI2020-01116). J.-H.J. is supported by the National Research Foundation of Korea (NRF) grant funded by the Korea government (MSIT) (NRF-2021R1A2C1011178).

Institutional Review Board Statement: Not applicable.

Informed Consent Statement: Not applicable.

Data Availability Statement: The data presented in this study are available on request from the corresponding author.

Acknowledgments: We thank the two anonymous reviewers and the editor for their constructive comments.

Conflicts of Interest: The authors declare that they have no conflict of interest.

References

1. Johannessen, O.M.; Kuzmina, S.I.; Bobylev, L.P.; Miles, M.W. Surface air temperature variability and trends in the Arctic: New amplification assessment and regionalisation. *Tellus A Dyn. Meteorol. Oceanogr.* **2016**, *68*, 28234. [CrossRef]
2. Serreze, M.C.; Barry, R.G. Processes and impacts of Arctic ampli fi cation: A research synthesis. *Glob. Planet. Chang.* **2011**, *77*, 85–96. [CrossRef]
3. Deser, C.; Walsh, J.E.; Timlin, M.S. Arctic Sea Ice Variability in the Context of Recent Atmospheric Circulation Trends. *J. Clim.* **2000**, *13*, 617–633. [CrossRef]
4. Lu, J.; Cai, M. Seasonality of polar surface warming amplification in climate simulations. *Geophys. Res. Lett.* **2009**, *36*, 1–6. [CrossRef]
5. Pithan, F.; Mauritsen, T. Arctic amplification dominated by temperature feedbacks in contemporary climate models. *Nat. Geosci.* **2014**, *7*, 2–5. [CrossRef]
6. Cohen, J.; Screen, J.A.; Furtado, J.C.; Barlow, M.; Whittleston, D.; Coumou, D.; Francis, J.; Dethloff, K.; Entekhabi, D.; Overland, J.; et al. Recent Arctic amplification and extreme mid-latitude weather. *Nat. Geosci.* **2014**, *7*, 627–637. [CrossRef]
7. Kug, J.-S.; Jeong, J.-H.; Jang, Y.-S.; Kim, B.-M.; Folland, C.K.; Min, S.-K.; Son, S.-W. Two distinct influences of Arctic warming on cold winters over North America and East Asia. *Nat. Geosci.* **2015**, *8*, 759–762. [CrossRef]
8. Screen, J.A.; Simmonds, I. Exploring links between Arctic amplification and mid-latitude weather. *Geophys. Res. Lett.* **2013**, *40*, 959–964. [CrossRef]
9. Wu, Y.; Smith, K.L. Response of Northern Hemisphere Midlatitude Circulation to Arctic Amplification in a Simple Atmospheric General Circulation Model. *J. Clim.* **2016**, *29*, 2041–2058. [CrossRef]
10. Boe, J.; Hall, A.; Qu, X. Current GCMs' Unrealistic Negative Feedback in the Arctic. *J. Clim.* **2009**, *22*, 4682–4695. [CrossRef]
11. de Boer, G.; Chapman, W.L.; Kay, J.E.; Medeiros, B.; Shupe, M.D.; Vavrus, S.; Walsh, J.E. A Characterization of the Present-Day Arctic Atmosphere in CCSM4. *J. Clim.* **2012**, *25*, 2676–2695. [CrossRef]
12. Karlsson, J.; Svensson, G. Consequences of poor representation of Arctic sea-ice albedo and cloud-radiation interactions in the CMIP5 model ensemble. *Geophys. Res. Lett.* **2013**, *40*, 4374–4379. [CrossRef]
13. Barton, N.P.; Klein, S.A.; Boyle, J.S. On the Contribution of Longwave Radiation to Global Climate Model Biases in Arctic Lower Tropospheric Stability. *J. Clim.* **2014**, *27*, 7250–7269. [CrossRef]
14. English, J.M.; Gettelman, A.; Henderson, G.R. Arctic radiative fluxes: Present-day biases and future projections in CMIP5 models. *J. Clim.* **2015**, *28*, 6019–6038. [CrossRef]

15. Baek, E.H.; Kim, J.H.; Park, S.; Kim, B.M.; Jeong, J.H. Impact of poleward heat and moisture transports on Arctic clouds and climate simulation. *Atmos. Chem. Phys.* **2020**, *20*, 2953–2966. [CrossRef]
16. Cesana, G.; Chepfer, H. How well do climate models simulate cloud vertical structure? A comparison between CALIPSO-GOCCP satellite observations and CMIP5 models. *Geophys. Res. Lett.* **2012**, *39*, 1–6. [CrossRef]
17. Kay, J.E.; Bourdages, L.; Miller, N.B.; Morrison, A.; Yettella, V.; Chepfer, H.; Eaton, B. Evaluating and improving cloud phase in the Community Atmosphere Model version 5 using spaceborne lidar observations. *J. Geophys. Res. Atmos.* **2016**, *121*, 4162–4176. [CrossRef]
18. Cesana, G.; Waliser, D.E.; Jiang, X.; Li, J.-L.F. Multi-model evaluation of cloud phase transition using satellite and reanalysis data. *J. Geophys. Res. Atmos.* **2015**, *120*, 7871–7892. [CrossRef]
19. English, J.M.; Kay, J.E.; Gettelman, A.; Liu, X.; Wang, Y.; Zhang, Y.; Chepfer, H. Contributions of clouds, surface albedos, and mixed-phase ice nucleation schemes to Arctic radiation biases in CAM5. *J. Clim.* **2014**, *27*, 5174–5197. [CrossRef]
20. Park, S.; Bretherton, C.S.; Rasch, P.J. Integrating Cloud Processes in the Community Atmosphere Model, Version 5. *J. Clim.* **2014**, *27*, 6821–6856. [CrossRef]
21. Tan, I.; Storelvmo, T. Sensitivity study on the influence of cloud microphysical parameters on mixed-phase cloud thermodynamic phase partitioning in CAM5. *J. Atmos. Sci.* **2016**, *73*, 709–728. [CrossRef]
22. Zhang, M.; Liu, X.; Diao, M.; D'Alessandro, J.J.; Wang, Y.; Wu, C.; Zhang, D.; Wang, Z.; Xie, S. Impacts of Representing Heterogeneous Distribution of Cloud Liquid and Ice on Phase Partitioning of Arctic Mixed-Phase Clouds with NCAR CAM5. *J. Geophys. Res. Atmos.* **2019**, *124*, 13071–13090. [CrossRef]
23. Danabasoglu, G.; Lamarque, J.F.; Bacmeister, J.; Bailey, D.A.; DuVivier, A.K.; Edwards, J.; Emmons, L.K.; Fasullo, J.; Garcia, R.; Gettelman, A.; et al. The Community Earth System Model Version 2 (CESM2). *J. Adv. Model. Earth Syst.* **2020**, *12*, e2019MS001916. [CrossRef]
24. McIlhattan, E.A.; Kay, J.E.; L'Ecuyer, T.S. Arctic Clouds and Precipitation in the Community Earth System Model Version 2. *J. Geophys. Res. Atmos.* **2020**, *125*, e2020JD032521. [CrossRef] [PubMed]
25. Larson, V.E. CLUBB-SILHS: A parameterization of subgrid variability in the atmosphere. *arXiv* **2017**, arXiv:1711.03675v2.
26. Bogenschutz, P.A.; Gettelman, A.; Morrison, H.; Larson, V.E.; Craig, C.; Schanen, D.P. Higher-order turbulence closure and its impact on climate simulations in the community atmosphere model. *J. Clim.* **2013**, *26*, 9655–9676. [CrossRef]
27. Morrison, H.; Gettelman, A. A New Two-Moment Bulk Stratiform Cloud Microphysics Scheme in the Community Atmosphere Model, Version 3 (CAM3). Part I: Description and Numerical Tests. *J. Clim.* **2008**, *21*, 3642–3659. [CrossRef]
28. Gettelman, A.; Morrison, H.; Santos, S.; Bogenschutz, P.; Caldwell, P.M. Advanced Two-Moment Bulk Microphysics for Global Models. Part II: Global model solutions and Aerosol-Cloud Interactions. *J. Clim.* **2015**, *28*, 1288–1307. [CrossRef]
29. Liu, X.; Ma, P.L.; Wang, H.; Tilmes, S.; Singh, B.; Easter, R.C.; Ghan, S.J.; Rasch, P.J. Description and evaluation of a new four-mode version of the Modal Aerosol Module (MAM4) within version 5.3 of the Community Atmosphere Model. *Geosci. Model Dev.* **2016**, *9*, 505–522. [CrossRef]
30. Beljaars, A.C.M.; Brown, A.R.; Wood, N. A new parametrization of turbulent orographic form drag. *Q. J. R. Meteorol. Soc.* **2004**, *130*, 1327–1347. [CrossRef]
31. Hurrell, J.W.; Hack, J.J.; Shea, D.; Caron, J.M.; Rosinski, J. A new sea surface temperature and sea ice boundary dataset for the community atmosphere model. *J. Clim.* **2008**, *21*, 5145–5153. [CrossRef]
32. Shaw, J.; McGraw, Z.; Bruno, O.; Storelvmo, T.; Hofer, S. Using Satellite Observations to Evaluate Model Microphysical Representation of Arctic Mixed-Phase Clouds. *Geophys. Res. Lett.* **2022**, *49*, e2021GL096191. [CrossRef]
33. Chepfer, H.; Bony, S.; Winker, D.; Cesana, G.; Dufresne, J.L.; Minnis, P.; Stubenrauch, C.J.; Zeng, S. The GCM-oriented CALIPSO cloud product (CALIPSO-GOCCP). *J. Geophys. Res. Atmos.* **2010**, *115*. [CrossRef]
34. Kay, J.E.; Hillman, B.R.; Klein, S.A.; Zhang, Y.; Medeiros, B.; Pincus, R.; Gettelman, A.; Eaton, B.; Boyle, J.; Marchand, R.; et al. Exposing global cloud biases in the Community Atmosphere Model (CAM) using satellite observations and their corresponding instrument simulators. *J. Clim.* **2012**, *25*, 5190–5207. [CrossRef]
35. Shaocheng, X.; McCoy, R.B.; Klein, S.A.; Cederwall, R.T.; Wiscombe, W.J.; Clothiaux, E.E.; Gaustad, K.L.; Golaz, J.C.; Hall, S.D.; Jensen, M.P.; et al. ARM climate modeling best estimate data: A new data product for climate studies. *Bull. Am. Meteorol. Soc.* **2010**, *91*, 13–20. [CrossRef]
36. Dee, D.P.; Uppala, S.M.; Simmons, A.J.; Berrisford, P.; Poli, P.; Kobayashi, S.; Andrae, U.; Balmaseda, M.A.; Balsamo, G.; Bauer, P.; et al. The ERA-Interim reanalysis: Configuration and performance of the data assimilation system. *Q. J. R. Meteorol. Soc.* **2011**, *137*, 553–597. [CrossRef]
37. Willis, M.D.; Leaitch, W.R.; Abbatt, J.P.D. Processes Controlling the Composition and Abundance of Arctic Aerosol. *Rev. Geophys.* **2018**, *56*, 621–671. [CrossRef]
38. Forbes, R.M.; Ahlgrimm, M. On the representation of high-latitude boundary layer mixed-phase cloud in the ECMWF global model. *Mon. Weather Rev.* **2014**, *142*, 3425–3445. [CrossRef]
39. Lenaerts, J.T.M.; Gettelman, A.; Van Tricht, K.; van Kampenhout, L.; Miller, N.B. Impact of Cloud Physics on the Greenland Ice.heet Near-Surface Climate: A Study with the Community Atmosphere Model. *J. Geophys. Res. Atmos.* **2020**, *125*, e2019JD031470. [CrossRef]
40. Hoose, C.; Kristjánsson, J.E.; Chen, J.P.; Hazra, A. A classical-theory-based parameterization of heterogeneous ice nucleation by mineral dust, soot, and biological particles in a global climate model. *J. Atmos. Sci.* **2010**, *67*, 2483–2503. [CrossRef]
41. Huang, Y.; Dong, X.; Kay, J.E.; Xi, B.; McIlhattan, E.A. The climate response to increased cloud liquid water over the Arctic in CESM1: A sensitivity study of Wegener–Bergeron–Findeisen process. *Clim. Dyn.* **2021**, *56*, 3373–3394. [CrossRef]